Supporting Information

Reducing Lifetime in Cu(I) Complexes with Thermally Activated Delayed Fluorescence and Phosphorescence promoted by Chalcogenolate-Diimine Ligand

Giliandro Farias[†], Cristian A.M. Salla[#], Renata S. Heying[†], Adailton J. Bortoluzi[†], Sergio F. Curcio[$], Thiago Cazati[$], Paloma L. dos Santos[&], Andrew P. Monkman[&], Bernardo de Souza[†*], Ivan H. Bechtold[#*]

*Corresponding authors: bernardo.souza@ufsc.br; tel: +55 48 37213608
ivan.bechtold@ufsc.br; tel: +55 48 37212304

[†]Department of Chemistry, Universidade Federal de Santa Catarina, 88040-900 Florianópolis, SC, Brazil

[#]Department of Physics, Universidade Federal de Santa Catarina, 88040-900 Florianópolis, SC, Brazil

[$]Department of Physics, Universidade Federal de Ouro Preto, 35400-000 Ouro Preto, MG, Brazil

[&]Department of Physics, Durham University, South Road, Durham, DH1 3LE, U.K.

INFRARED SPECTROSCOPY

Scheme S1. Synthesis route to obtain complexes **C1-C2**. The route for **S1**, **S2**, **Se1** and **Se2** follows the same method but the ligand phenanthroline is substituted by TDZP or PhenSe ligands.

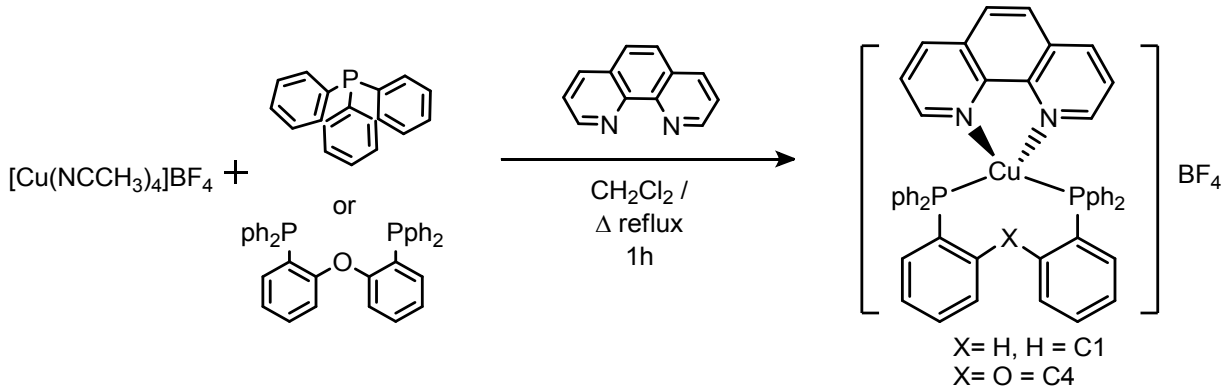

Table S1. Attributions of IR bands for complexes **C1-Se2**.

	C1	**S1**	**Se1**	**C2**	**S2**	**Se2**
ν (C-Har)	3057 – 2862	3057	3050 – 2849	3058 – 2954	3050	3064 – 2856
ν (C=N e C=C)	1670 – 1432	1585 – 1399	1599 – 1399	1768 – 1435	1566 – 1405	1566 – 1434
ν (C–O)	-	-	-	1207	1212	1212
ν (B–F)	1055	1053	1059	1054	1053	1059
δ (C-Har)	843 - 510	817 - 515	816 - 512	846 – 513	816 – 497	872 – 512

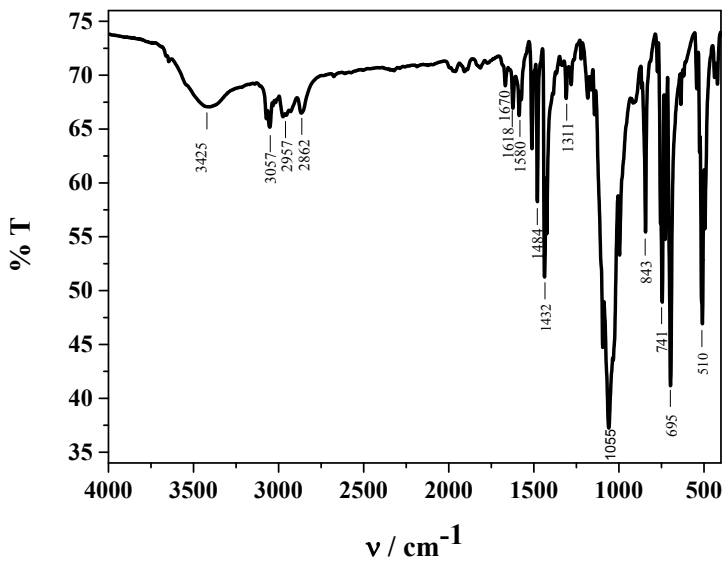

Figure S1. IR spectra of the complex **C1** in KBr pellet.

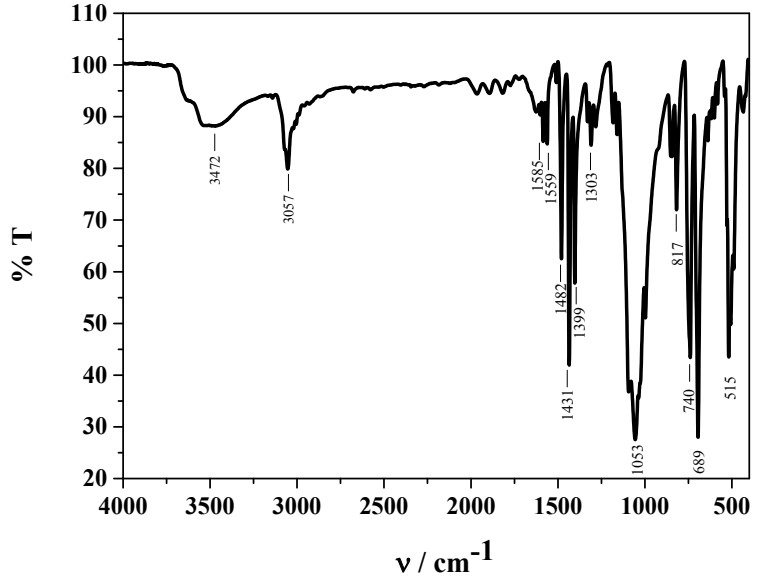

Figure S2. IR spectra of the complex **S1** in KBr pellet.

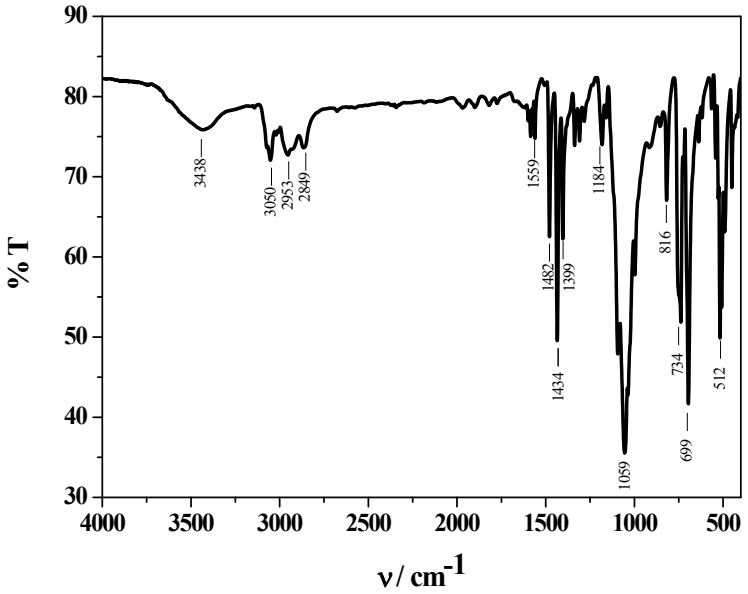

Figure S3. IR spectra of the complex **Se1** in KBr pellet.

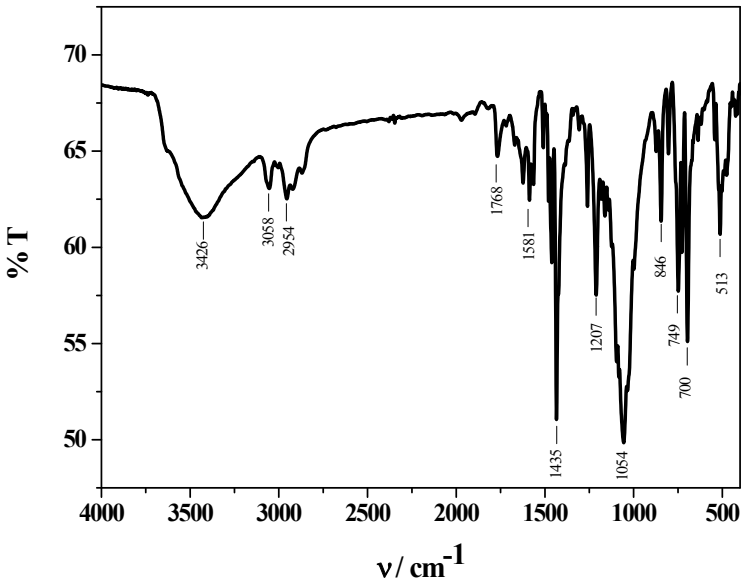

Figure S4. IR spectra of the complex **C2** in KBr pellet.

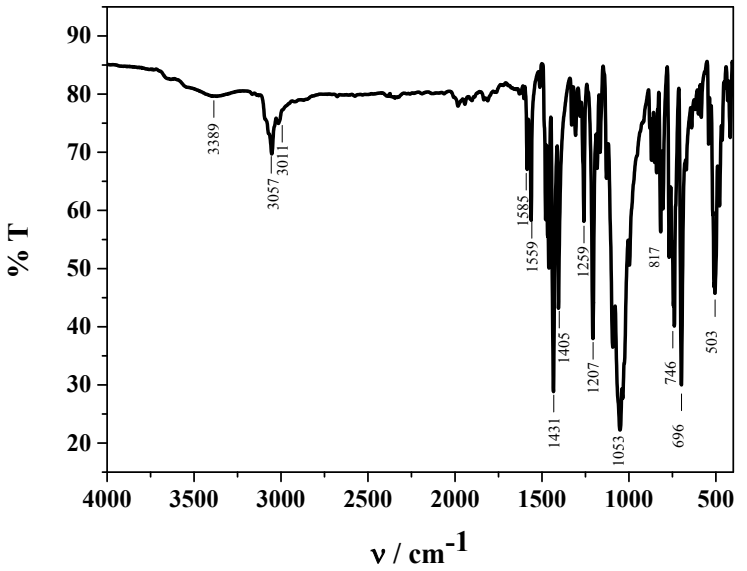

Figure S5. IR spectra of the complex **S2** in KBr pellet.

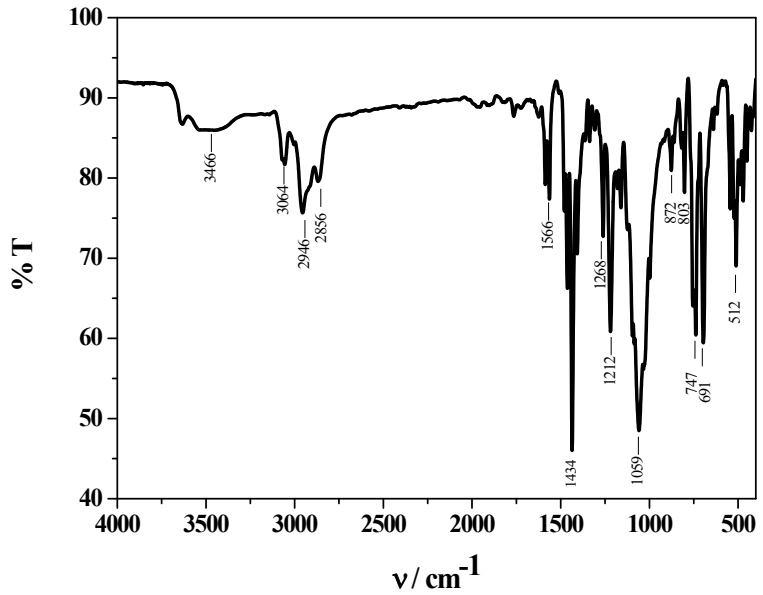

Figure S6. IR spectra of the complex **Se2** in KBr pellet.

THERMOGRAVIMETRIC ANALYSIS AND CYCLIC VOLTAMMETRY

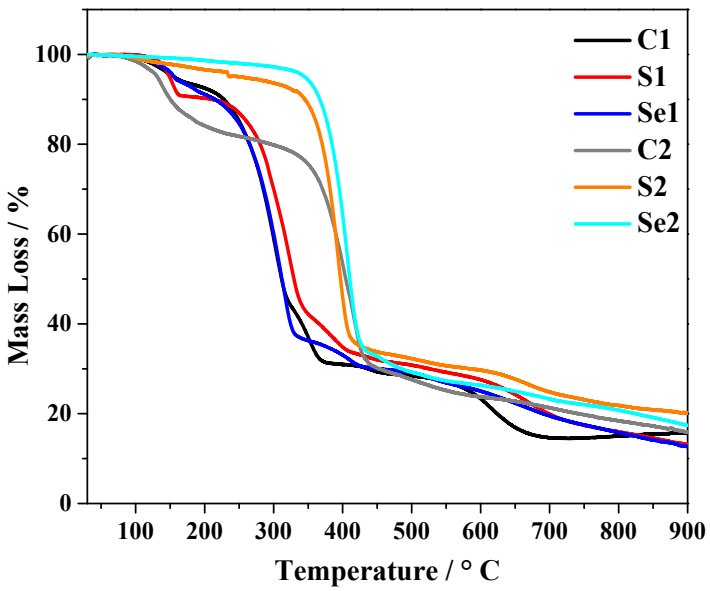

Figure S7. C1-Se2 thermogravimetric analysis (TGA) using a heating ramp of 10 ^{o}C min^{-1} under nitrogen atmosphere.

UV-VIS ABSORTION IN PMMA AND EMISSION IN SOLUTION

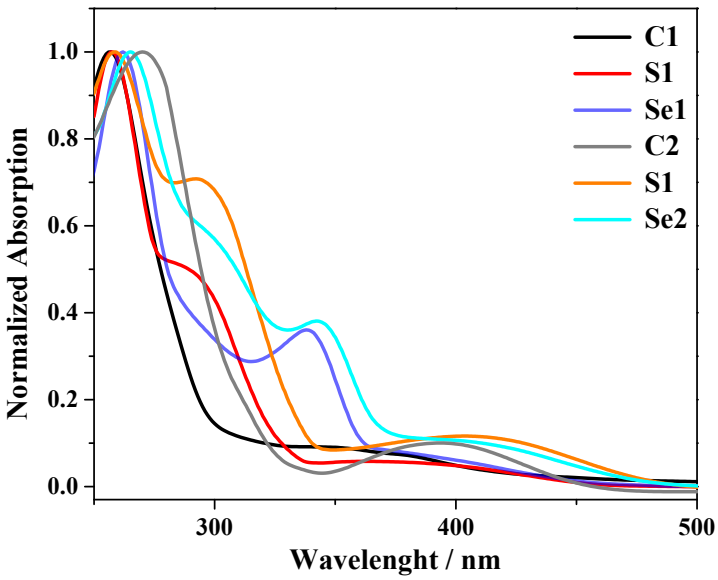

Figure S8. Optical absorption spectra of the Cu(I) complexes in 10 wt% in PMMA.

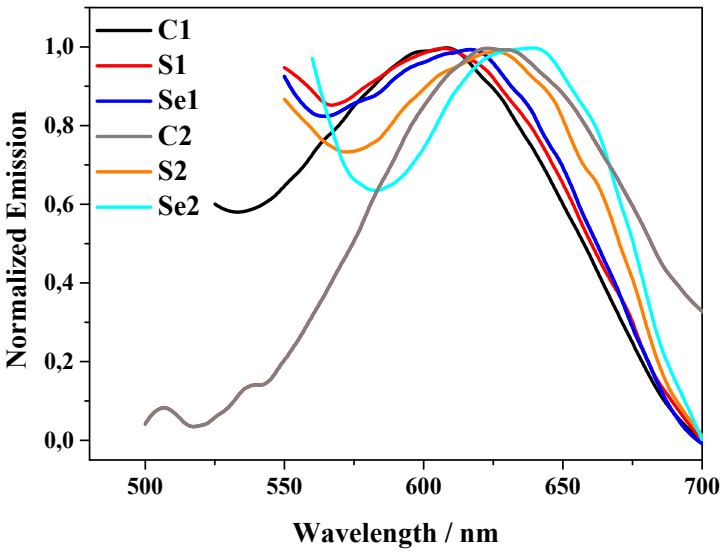

Figure S9. Emission spectra obtained by excitation at the low energy region of the first absorption of the copper(I) complexes in CH_2Cl_2 solution 1.0×10^{-5} mol L^{-1}.

Table S2. Optical absorption data for the Cu(I) complexes in CH_2Cl_2 solution 1.0×10^{-5} mol L^{-1}.

Complex	λ_{max} / nm (ε / mol^{-1} L cm^{-1})
C1	257 (25.024) , 352 (2.772)
S1	260 (39.823), 286[a], 370 (1.808)
Se1	265 (57.389), 340(20.877)
C2	269 (38.620) , 391 (2.840)
S2	259 (59.894), 291 (33.653), 404 (3.881)
Se2	264 6.566), 341 (16.354), 396 (4.252)

TIME-CORRELATED SINGLE-PHOTON COUNTING AND FITTING

The emission decays at maxima emission of the Cu(I) complexes 10 wt% in PMMA (see Figure S19) were best fitted by a bi-exponential function. The excited state lifetimes and their relative amplitudes are showed in Table S4 (see ESI). The longer lifetimes (τ_1), in the range of 2.7 μs to 800 ns, were attributed to delayed fluorescence emission, whilst the shorter lifetimes (τ_2) ranging from 20 to 90 ns were attributed to the prompt fluorescence emission.

Table S3. Excited-state lifetimes and their relative amplitudes of the Cu (I) complexes dispersed 10 wt% in PMMA measured at maximum emission wavelength.

	τ_1 (μs)	A_1(%)	τ_2 (μs)	A_2(%)	χ^2
C1	2.7±0.2	64.21	0.02±0.01	35.79	1.022
S1	1.2±0.7	58.53	0.08±0.01	41.47	0.940
Se1	1.1±0.5	38.27	0.09±0.01	61.73	0.974
C2	2.2±0.1	73.37	0.08±0.01	26.63	0.964
S2	1.2±0.1	68.33	0.07±0.01	31.67	0.934
Se2	0.8±0.1	48.60	0.07±0.01	51.40	0.943

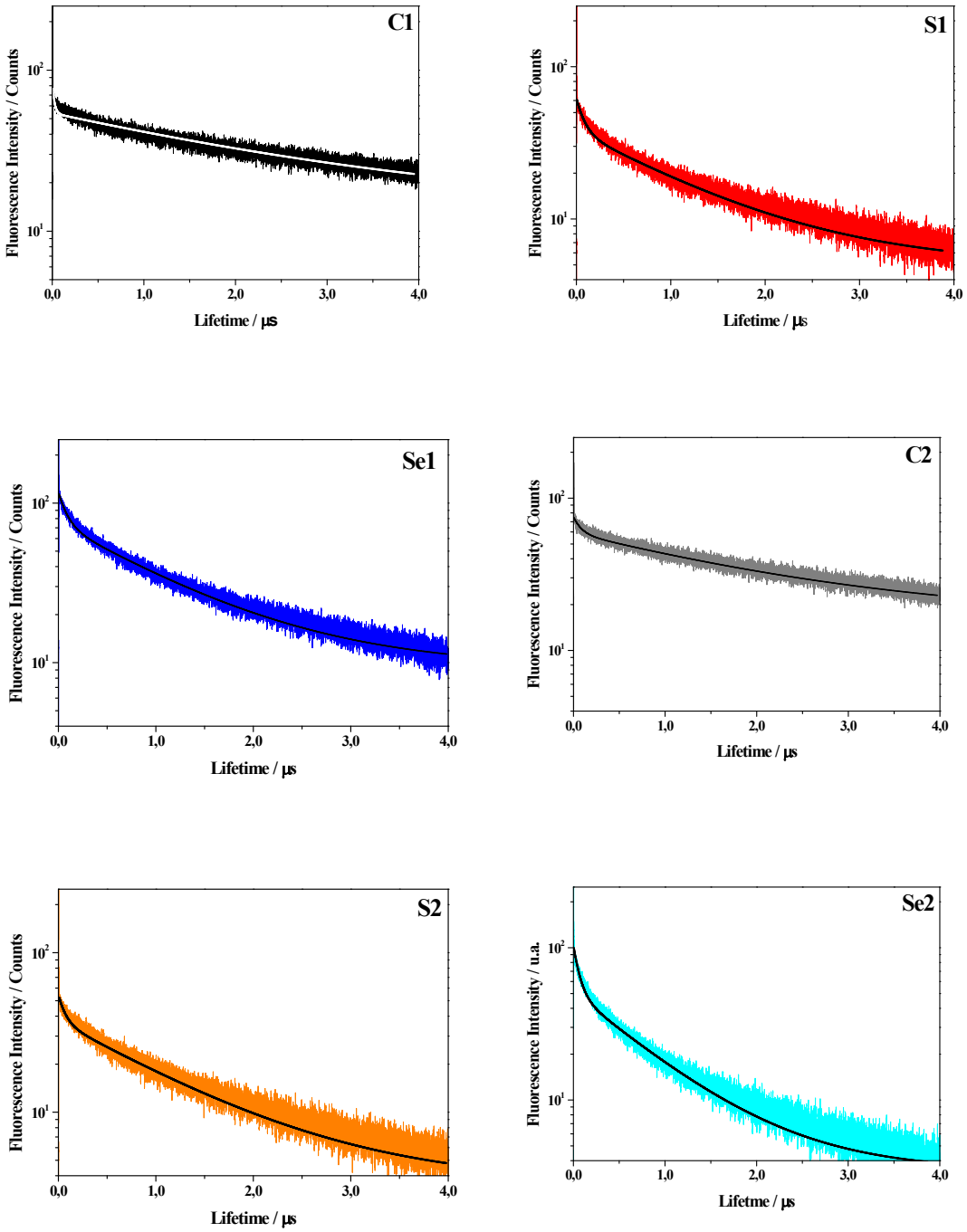

Figure S10. Emission decay curves of the Cu (I) complexes dispersed 10 wt% in PMMA fitted with a bi-exponential function,

TIME RESOLVED EMISSION SPECTRA

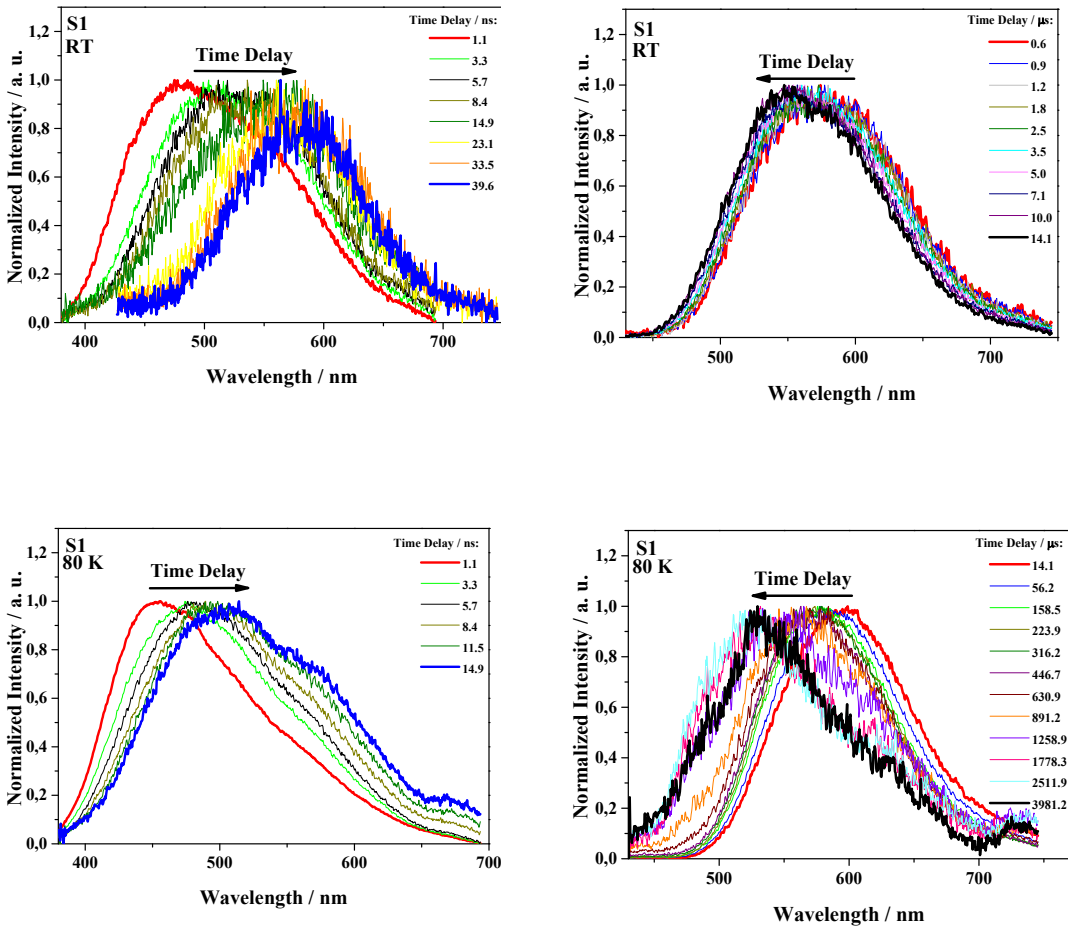

Figure S11. Time resolved normalized emission spectra at room temperature (up) and 80K (down) for **S1** 10 wt% in PMMA. Films were excited at 355 nm.

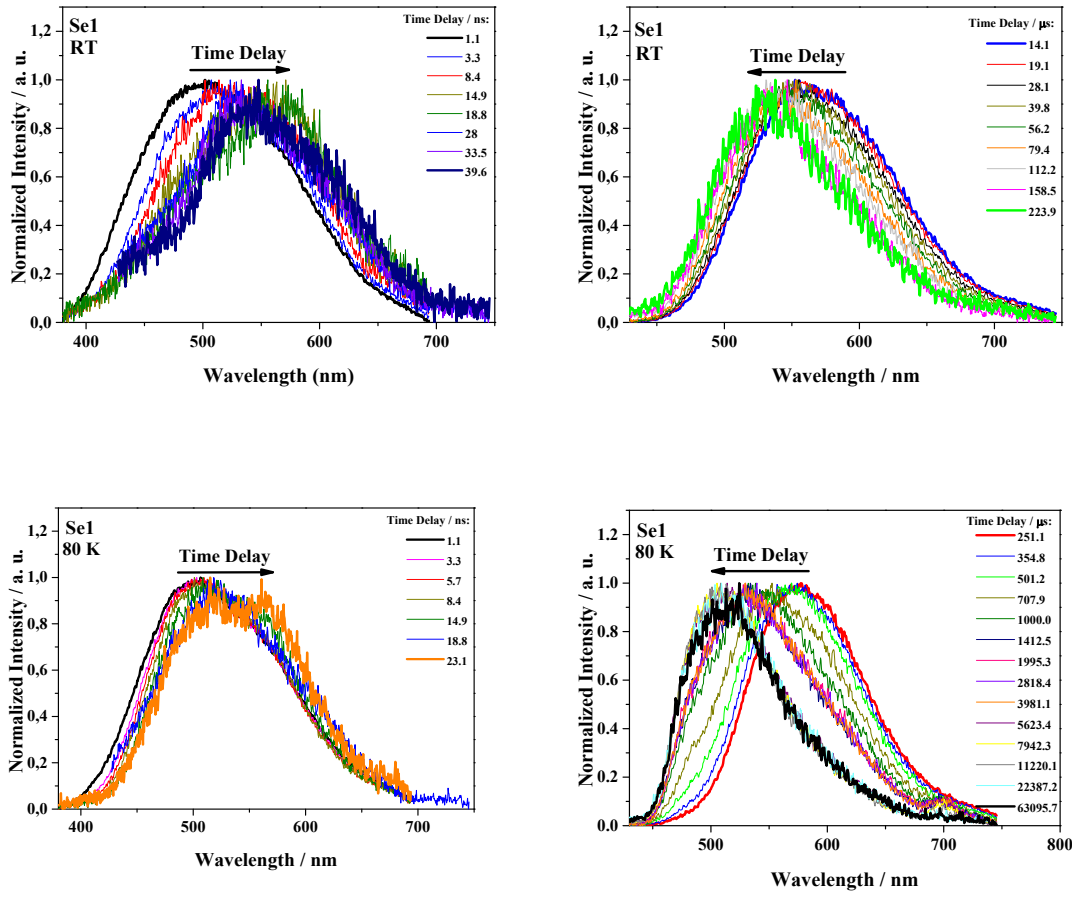

Figure S12. Time resolved normalized emission spectra at room temperature (up) and 80K (down) for **Se1** 10 wt% in PMMA. Films were excited at 355 nm.

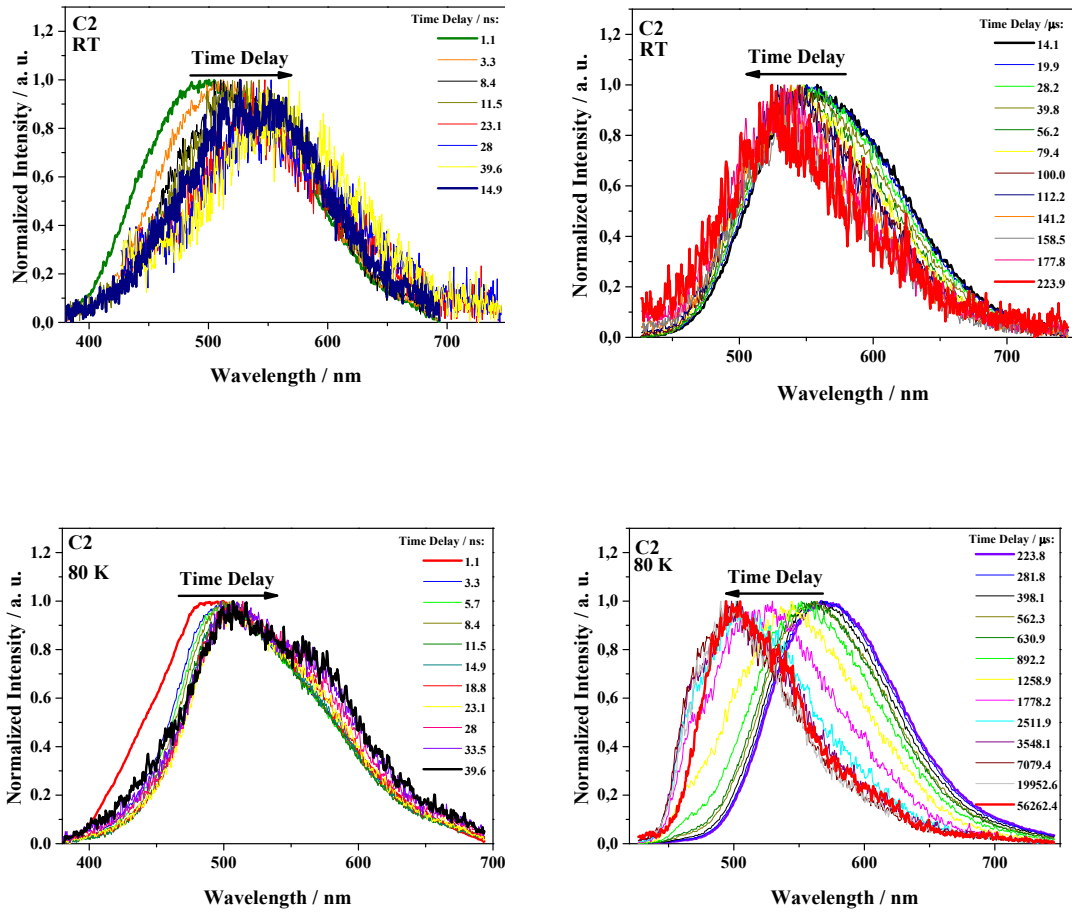

Figure S13. Time resolved normalized emission spectra at room temperature (up) and 80K (down) for **C2** 10 wt% in PMMA. Films were excited at 355 nm.

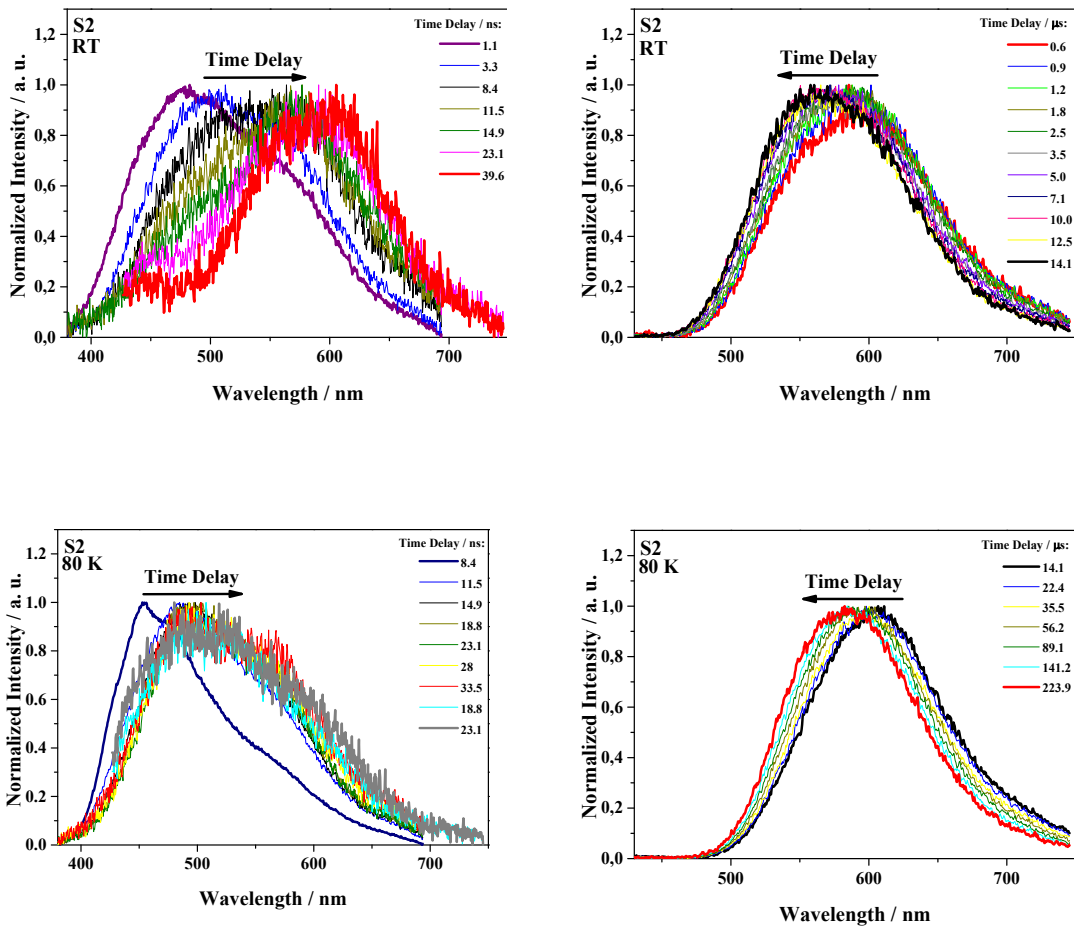

Figure S14. Time resolved normalized emission spectra at room temperature (up) and 80K (down) for **S2** 10 wt% in PMMA. Films were excited at 355 nm.

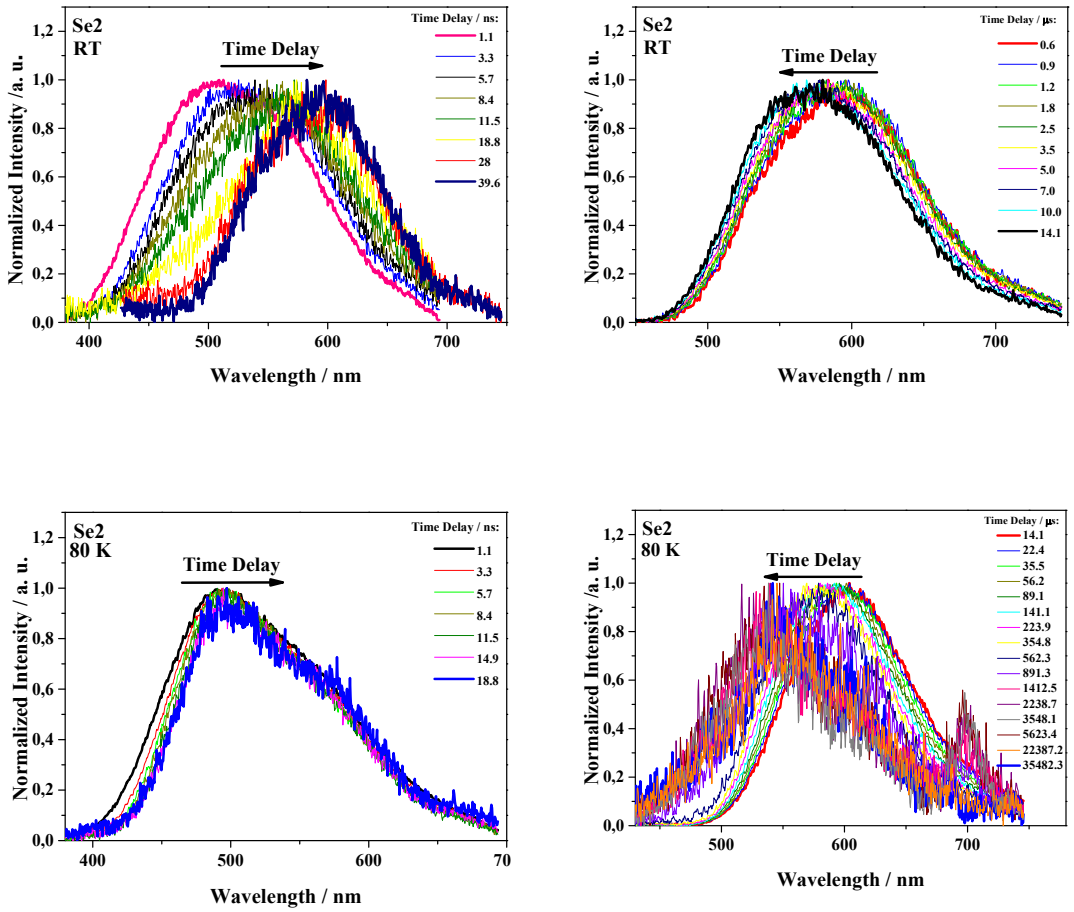

Figure S15. Time resolved normalized emission spectra at room temperature (up) and 80K (down) for **Se2** 10 wt% in PMMA. Films were excited at 355 nm.

THEORICAL MODELING

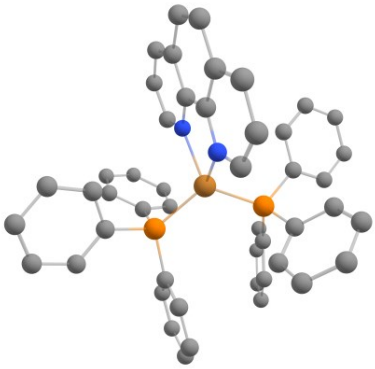

C1

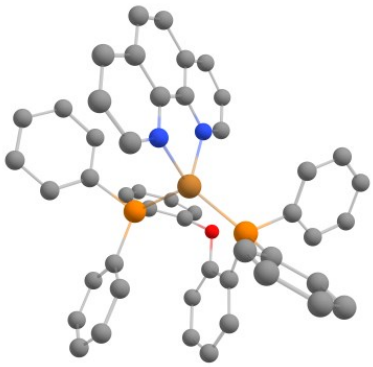

C2

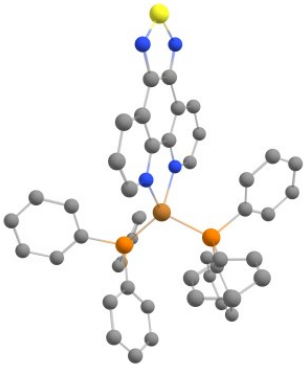

S1

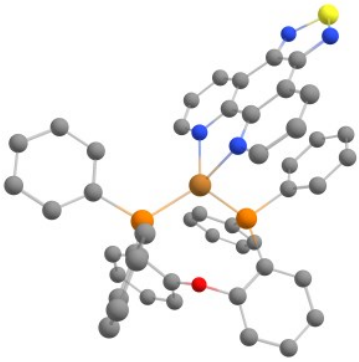

S2

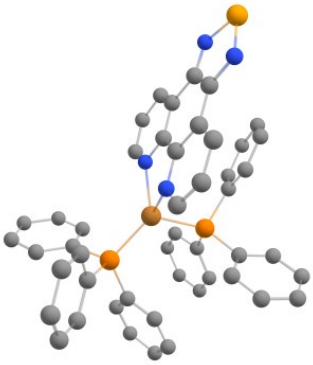

Se1

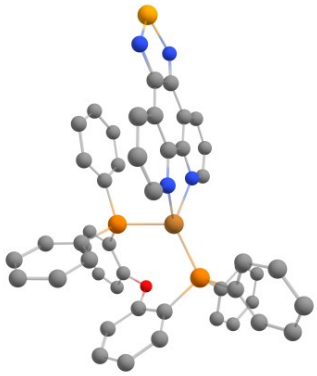

Se2

Figure S16. Optimized geometry for complexes **C1-Se2** obtained from DFT using PBE0/def2-TZVP(-f).

Table S4. Selected bond lengths (Å), bond angles (°) at optimized S_0 geometry for complexes **C1-Se2** using PBE0/def2-TZVP(-f).

	C1		**C2**	
	Exp	**S_0**	**Exp**	**S_0**
Cu-N1	2.080	2.122	2.071	2.091
Cu-N10	2.070	2.115	2.063	2.081
Cu-P1	2.271	2.272	2.261	2.284
Cu-P2	2.245	2.268	2.231	2.227
Cu···O	-	-	3.205	3.082
N1-Cu-N10	80.90	79.20	80.83	80.52
P1-Cu-N1	115.44	106.15	110.81	102.87
P2-Cu-P1	118.69	114.33	108.12	114.25
N10-Cu-P2	103.60	106.15	109.08	133.34
	S1			
	Exp	**S_0**	**Exp**	**S_0**
Cu-N1	2.082	2.123	2.058	2.064
Cu-N10	2.087	2.095	2.071	2.062
Cu-P1	2.258	2.271	2.254	2.276
Cu-P2	2.266	2.266	2.223	2.221
Cu···O	-	-	3.039	3.120
N1-Cu-N10	80.01	79.048	80.75	81.35
P1-Cu-N1	117.88	126.66	105.87	99.93
P2-Cu-P1	116.15	113.45	112.57	117.07
N10-Cu-P2	112.67	113.44	119.99	132.82
	Se1		**Se2**	
	Exp	**S_0**	**Exp**	**S_0**
Cu-N1	2.087	2.104	2.070	2.093
Cu-N10	2.088	2.095	2.040	2.156
Cu-P1	2.263	2.301	2.256	2.327
Cu-P2	2.273	2.246	2.219	2.243
Cu···O	-	-	3.105	3.296
N1-Cu-N10	79.93	79.72	81.11	78.58
P1-Cu-N1	111.09	101.10	107.31	101.97
P2-Cu-P1	115.75	114.98	117.47	115.02
N10-Cu-P2	113.68	124.91	110.73	124.83

Table S5. Data for the TD-DFT excitations using PBE0/def2-TZVP(-f) for complexes **C1** and **C2**.

State[a]	Energy [b] eV	Energy [b] nm	f [b]	Configuration (%) [c]	Assingment
			C1		
T_1	2.43	511	2.096×10^{-6}	H → L (91)	d(Cu)+π(PPh_3) → π*(phen)
T_2	2.83	437	7.267×10^{-6}	H → L+1 (62) H-3 → L+1 (28)	d(Cu)+π(PPh_3) → π*(phen) π(phen) → π*(phen)
T_3	2.96	418	3.035×10^{-4}	H-2 → L (88)	d(Cu)+π(PPh_3) → π*(phen)
S_1	2.78	446	0.0870	H → L (90)	d(Cu)+π(PPh_3) → π*(phen)
S_2	2.84	436	0.0086	H → L+1 (95)	d(Cu)+π(PPh_3) → π*(phen)
S_3	3.15	393	0.0200	H-2 → L (89)	d(Cu)+π(PPh_3) → π*(phen)
S_4	3.24	382	0.0095	H-1 → L (94)	d(Cu)+π(PPh_3) → π*(phen)
			C2		
T_1	2.43	512	2.131×10^{-6}	H → L (93)	d(Cu)+π(PPh_3) → π*(phen)
T_2	2.76	449	1.310×10^{-4}	H → L+1 (67) H-4 → L+1 (22)	d(Cu)+π(PPh_3) → π*(phen) π(phen) → π*(phen)
T_3	2.83	438	0.0043	H-1 → L (70) H-2 → L (20)	d(Cu)+π(PPh_3) → π*(phen) d(Cu)+π(PPh_3) → π*(phen)
S_1	2.80	443	0.0778	H → L (89)	d(Cu)+π(PPh_3) → π*(phen)
S_2	2.82	440	0.0123	H → L+1 (96)	d(Cu)+π(PPh_3) → π*(phen)
S_3	3.05	406	0.0187	H-1 → L (80)	d(Cu)+π(PPh_3) → π*(phen)
S_4	3.32	373	0.0025	H-1 → L+1 (57) H-2 → L (22) H-2 → L+1 (11)	d(Cu)+π(PPh_3) → π*(phen) d(Cu)+π(PPh_3) → π*(phen) d(Cu)+π(PPh_3) → π*(phen)

[a] Vertical states taking S_0 geometry as reference; [b] Values obtained for the triplet states are shown as an average of the substates x, y and z; [c] Transitions with high percentage contributions are shown in parenthesis.

Table S6. Data for the TD-DFT excitations using PBE0/def2-TZVP(-f) for complexes **S1** and **S2**.

State[a]	Energy [b] eV	Energy [b] nm	f [b]	Configuration (%) [c]	Assingment
				S1	
T_1	2.10	591	4.076×10^{-7}	H → L (65) H → L+1 (25)	d(Cu)+π(PPh_3) → π*(thiadiazol) d(Cu)+π(PPh_3) → π*(phen)
T_2	2.24	555	1.774×10^{-6}	H → L+1 (67) H → L (28)	d(Cu)+π(PPh_3) → π*(phen) d(Cu)+π(PPh_3) → π*(thiadiazol)
T_3	2.86	467	0.0023	H-2 → L (13) H-2 → L+1 (56) H-1 → L+1 (11)	d(Cu)+π(PPh_3) → π*(thiadiazol) d(Cu)+π(PPh_3) → π*(phen) d(Cu)+π(PPh_3) → π*(phen)
S_1	2.34	528	0.0367	H → L (90)	d(Cu)+π(PPh_3) → π*(thiadiazol)
S_2	2.75	452	0.0636	H → L+1 (83)	d(Cu)+π(PPh_3) → π*(phen)
S_3	2.98	416	0.0095	H-2 → L (32) H-2 → L+1 (29) H-1 → L (17) H-1 → L+1 (15)	d(Cu)+π(PPh_3) → π*(thiadiazol) d(Cu)+π(PPh_3) → π*(phen) d(Cu)+π(PPh_3) → π*(thiadiazol) d(Cu)+π(PPh_3) → π*(phen)
S_4	3.07	404	0.0114	H → L+2 (83)	d(Cu)+π(PPh_3) → π*(phen)
				S2	
T_1	2.33	533	1.137×10^{-6}	H → L (35) H → L+1 (61)	d(Cu)+π(PPh_3) → π*(thiadiazol) d(Cu)+π(PPh_3) → π*(phen)
T_2	2.36	525	0.949×10^{-6}	H → L (52) H → L+1 (30)	d(Cu)+π(PPh_3) → π*(thiadiazol) d(Cu)+π(PPh_3) → π*(phen)
T_3	2.82	473	0.0007	H-2 → L (13) H-2 → L+1 (63)	d(Cu)+π(PPh_3) → π*(thiadiazol) d(Cu)+π(PPh_3) → π*(phen)
S_1	2.45	505	0.0335	H → L (88)	d(Cu)+π(PPh_3) → π*(thiadiazol)
S_2	2.80	443	0.0407	H → L+1 (86)	d(Cu)+π(PPh_3) → π*(phen)
S_3	2.94	421	0.0012	H-2 → L (43) H-2 → L+1 (48)	d(Cu)+π(PPh_3) → π*(thiadiazol) d(Cu)+π(PPh_3) → π*(phen)
S_4	3.15	411	0.0076	H-1 → L (53) H-1 → L+1 (34)	d(Cu)+π(PPh_3) → π*(thiadiazol) d(Cu)+π(PPh_3) → π*(phen)

[a] Vertical states taking S_0 geometry as reference; [b] Values obtained for the triplet states are shown as an average of the substates x, y and z; [c] Transitions with high percentage contributions are shown in parenthesis.

Table S7. Data for the TD-DFT excitations using PBE0/def2-TZVP(-f) for complexes **Se1** and **Se2**.

State[a]	Energy [b] eV	Energy [b] nm	f [b]	Configuration (%) [c]	Assingment
				Se1	
T_1	1.98	625	9.766×10^{-7}	H → L (83)	d(Cu)+π(PPh_3) → π*(selenodiazol)
T_2	2.39	520	5.996×10^{-7}	H → L+1 (82)	d(Cu)+π(PPh_3) → π*(selenodiazol)
T_3	2.83	449	0.0003	H-4 → L (61) H → L (10)	π(PPh_3) → π*(selenodiazol) d(Cu)+π(PPh_3) → π*(selenodiazol)
S_1	2.30	538	0.0128	H → L (96)	d(Cu)+π(PPh_3) → π*(selenodiazol)
S_2	2.82	439	0.0989	H → L+1 (93)	d(Cu)+π(PPh_3) → π*(phen)
S_3	2.98	416	7.180×10^{-5}	H-2 → L (44) H-2 → L+1 (26) H-1 → L (20)	d(Cu)+π(PPh_3) → π*(selenodiazol) d(Cu)+π(PPh_3) → π*(phen) d(Cu)+π(PPh_3) → π*(selenodiazol)
S_4	3.00	413	0.0119	H-2 → L (17) H-1 → L (63)	d(Cu)+π(PPh_3) → π*(selenodiazol) d(Cu)+π(PPh_3) → π*(selenodiazol)
				Se2	
T_1	2.24	555	7.946×10^{-7}	H → L (76)	d(Cu)+π(PPh_3) → π*(selenodiazol)
T_2	2.45	507	8.276×10^{-7}	H → L+1 (87)	d(Cu)+π(PPh_3) → π*(phen)
T_3	2.81	467	0.0004	H-2 → L (18) H-1 → L (41) H → L (22)	d(Cu)+π(PPh_3) → π*(selenodiazol) d(Cu)+π(PPh_3) → π*(selenodiazol) d(Cu)+π(PPh_3) → π*(selenodiazol)
S_1	2.13	536	0.0251	H → L (93)	d(Cu)+π(PPh_3) → π*(selenodiazol)
S_2	2.79	444	0.0531	H → L+1 (91)	d(Cu)+π(PPh_3) → π*(phen)
S_3	2.90	427	0.0001	H-2 → L (42) H-2 → L+1 (36) H-1 → L (11)	d(Cu)+π(PPh_3) → π*(selenodiazol) d(Cu)+π(PPh_3) → π*(phen) d(Cu)+π(PPh_3) → π*(selenodiazol)
S_4	2.94	422	0.0071	H-2 → L (13) H-1 → L (57) H-1 → L+1 (17)	d(Cu)+π(PPh_3) → π*(selenodiazol) d(Cu)+π(PPh_3) → π*(selenodiazol) d(Cu)+π(PPh_3) → π*(phen)

[a] Vertical states taking S_0 geometry as reference; [b] Values obtained for the triplet states are shown as an average of the substates x, y and z; [c] Transitions with high percentage contributions are shown in parenthesis.

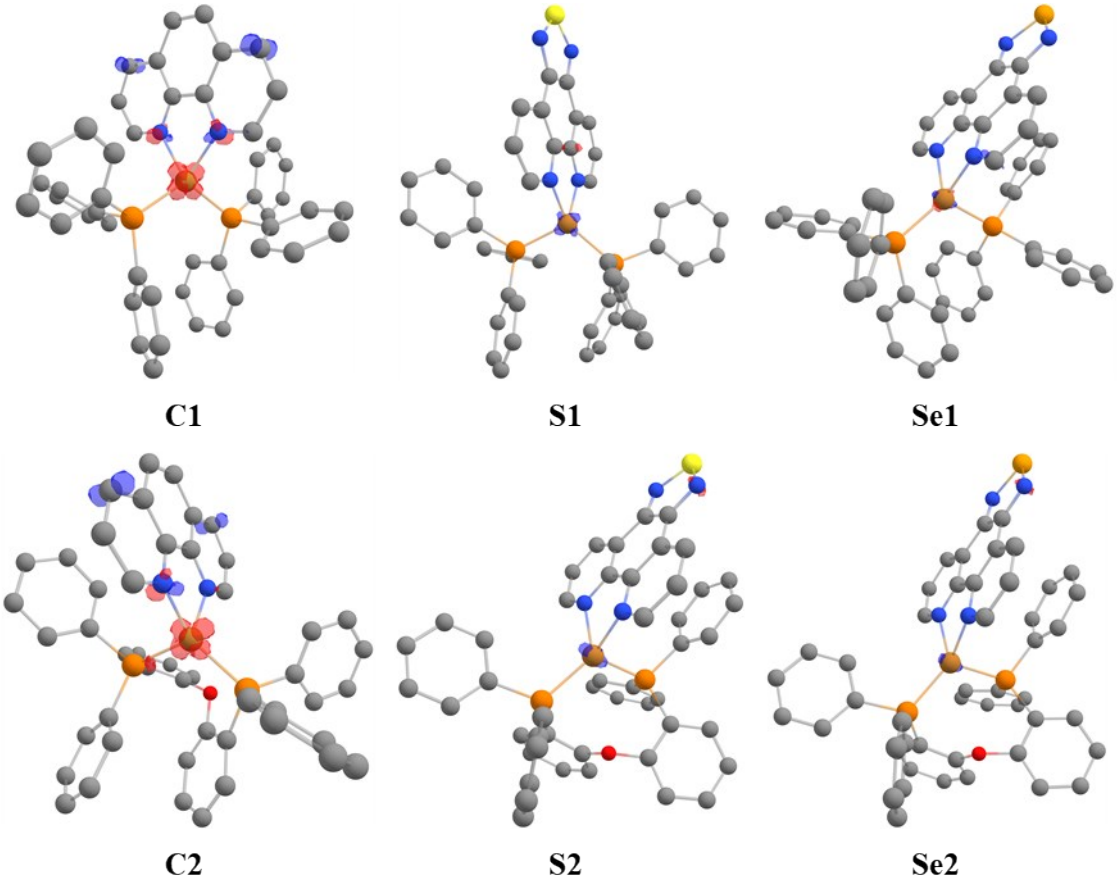

Figure S17. Multiplied HOMO and LUMO orbitals of **C1-Se2** to show their overlap. As one can see the overlap which is mainly centered at copper atom is reduced from **C1** to **Se1** and from **C2** to **Se2**. The isosurface was increased by a factor of 10 times in comparison to those of the molecular orbitals in Figure 5.

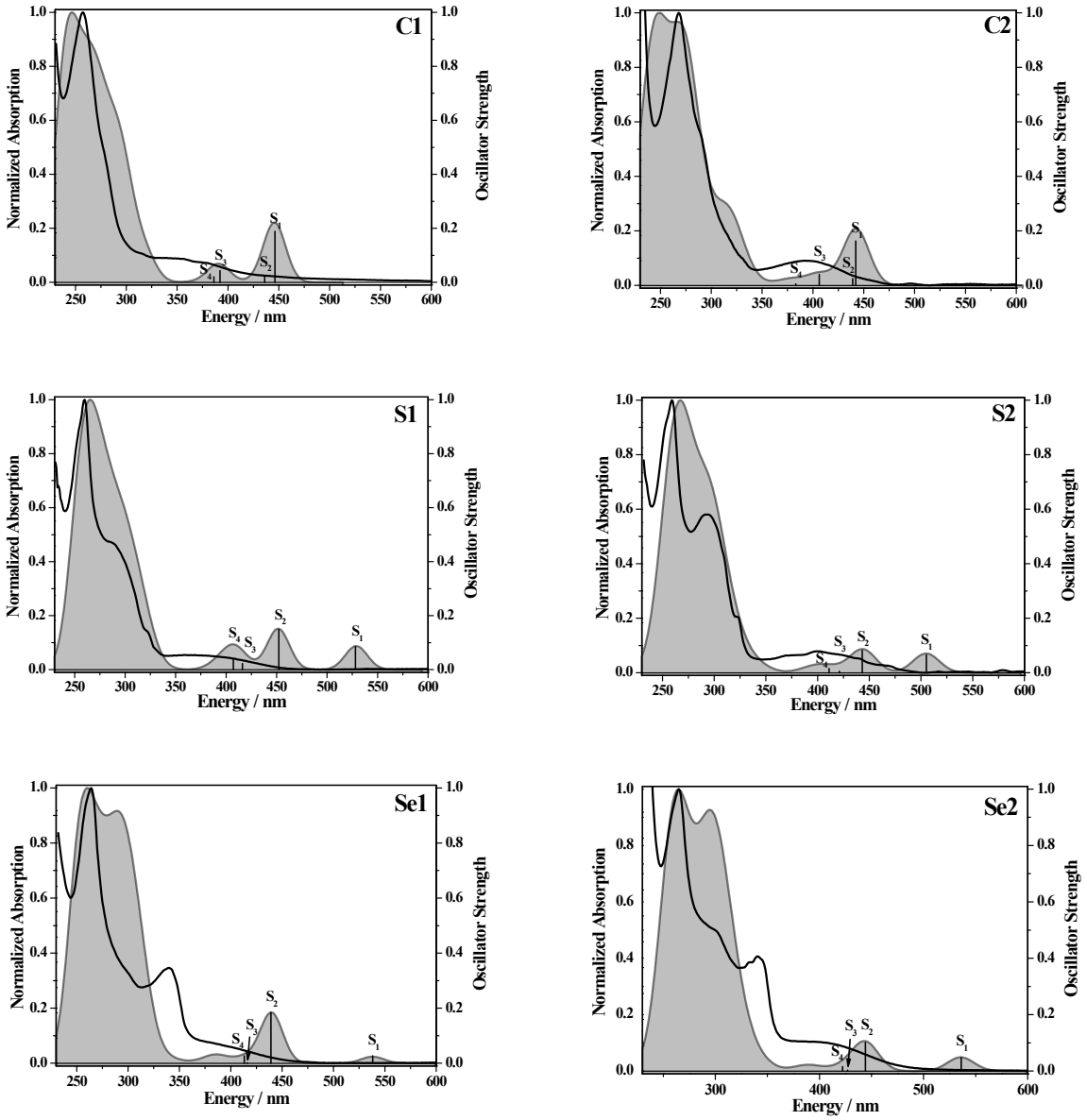

Figure S18. Experimental absorption spectra of **C1-Se2** in CH_2Cl_2 and the theoretical absorption spectra (filled curves) calculated using PBE0/def2-TZVP(-f) and convoluted with Gaussians of 0.15 eV width.

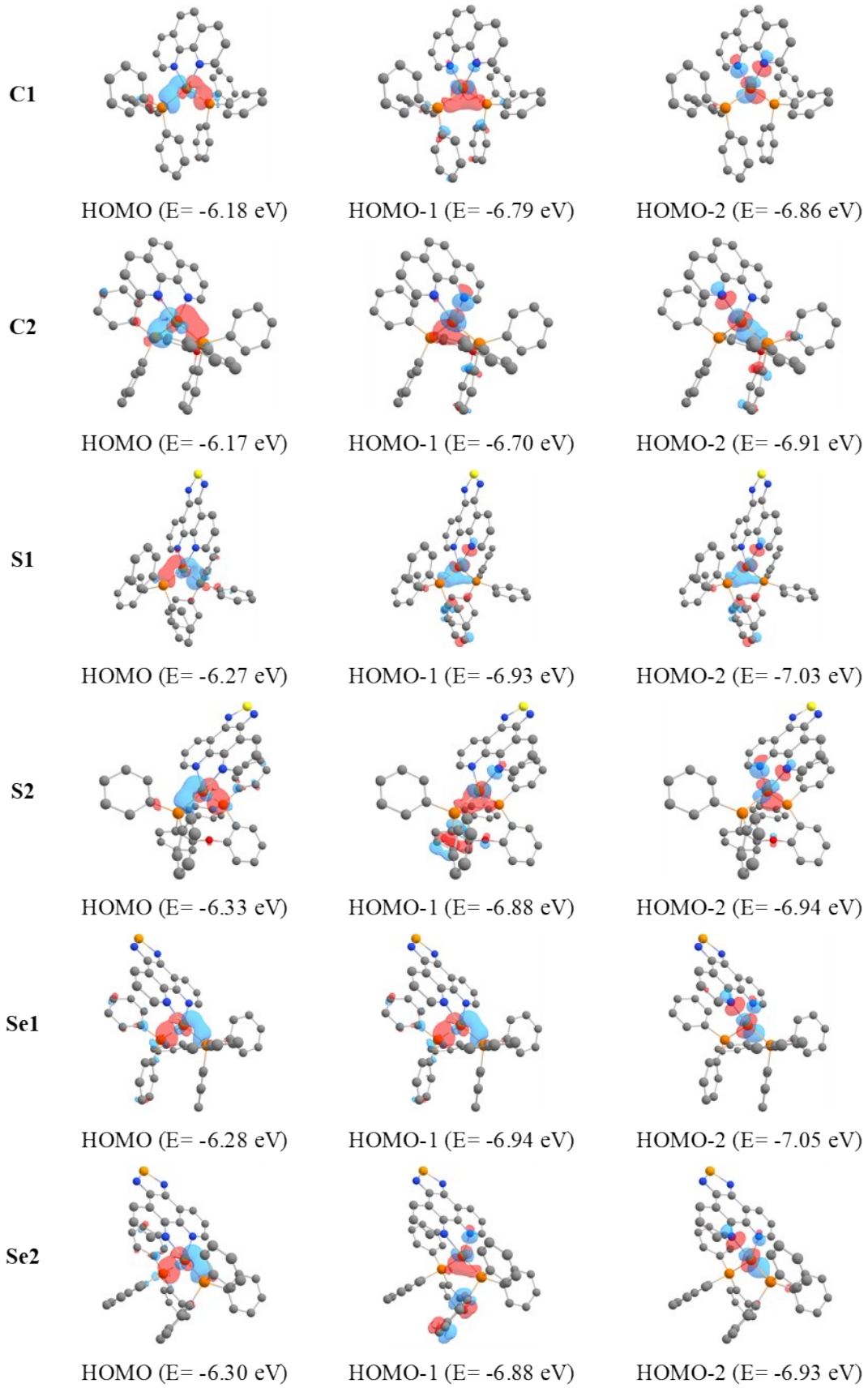

Figure S19. HOMO, HOMO-1 and HOMO-2 orbitals of complexes **C1–Se2** and their energies calculated using PBE0/def2-TZVP(-f).